# Conceptual Design of An Aircraft Wing: Integration Management of Meso Structures in Passive Morphing Airfoils

**Cedric Dave D. Montecillo, Yakub Mogul, *Muhammad Azeem, Asma Begum, Ibtisam Mogul, Ayesha Adeel**
University of Bolton RAK Academic Center, Ras Al Khaimah, UAE
*Correspondence email: drazeemhr@gmail.com

## Abstract
The aim of this study is to study and examine the behavioral characteristics of an airfoil integrated with Meso-structures, such as re-entrant or auxetic structure, a regular honeycomb and hybrid honeycomb. Understanding them through different analysis such as structural and computational fluid dynamics that will supplement the fluid-structure interaction, simulating the airfoil configurations under different static and working conditions such as different angles of attack that will simulate cruising and takeoff conditions. The results show that the desirable material for large deformation during flights is the GFRP material and the safer and more stable configuration is the Hybrid Honeycomb.

**Key words**: Airfoil, Meso-structures, Morphing wing, Concept wing design, Aerodynamic loads, Fluid-structure interactions (FSI)

## 1. Introduction
The need for a more efficient airfoil is being in demand as the increase in need for structures that can provide aerodynamic efficiency that can lead to fuel efficiency. Regular wings have too much complex components that try to adapt to the specific conditions of the mission, and different planes are created for specific mission conditions which is inefficient and the need for a much more adaptable aircraft is prevalent. This paper is focuses on the morphing airfoil, which is an airfoil that is the result of the research of how birds fly to improve man-made aircrafts, understanding that birds can alter their wing shape to achieve maneuverability and the maximum performance in different flight conditions (Spadoni & Ruzzene 2007)., a decade ago, a concept of a morphing wing was introduced, which can have a fully deformable airfoil section that can adapt to various flight conditions during flight. Several tests and experiments showed that the type of morphing the morphing wing possess can provide aerodynamic benefits to an aircraft. Which is then integrated with Meso-structures (Gibson & Ashby 2010), or cellular structures are being subject to increased interests and applications due to their excellent properties both mechanical and light weight characteristics, this is highly relevant to the aircraft and aerospace industry due to the need for certain applications requiring being both stronger and light structures. (Yang & Chang, 2013), Honeycomb structures are much prevalent, in consideration of the desire for stronger and light weight structural materials for the said industries, which pushed the development of the honeycombs for technological use.
The configurations or patterns include the regular honeycomb, auxetic honeycomb and hybrid honeycomb, and the study will also include the comparison of two different materials, Al 6061 T6 and the Glass fiber reinforced polymer. The patterns are all cellular structures, one having a "+" Poisson's ratio, a "- "Poisson's ratio and a "0" Poisson's ratio, comparing their behavior against static loads, and aerodynamic loads, finding which of them is a much suitable fit for the morphing airfoil application. The two different materials are applied to all configurations throughout the analysis. The study that will be conducted will be mainly focused on the Fluid-structure interaction, whereas the structural and the computational fluid dynamics will supplement the FSI.

## 2. Literature Review
### 2.1. Airfoil
An airfoil is a device that utilizes the flow of air over its surface, which is possible when an airfoil is moved through the air, it produces lift.

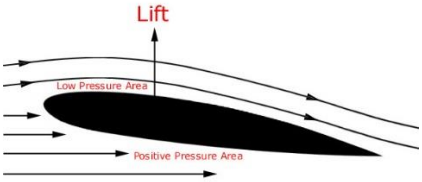


Figure 1. Aerofoil and Lifts (Airfoils 2019)
It is constructed to have air flow more rapidly on the upper surface and slower on the lower surface, this allows the pressure to be low on the upper surface but have high pressure on the lower surface.

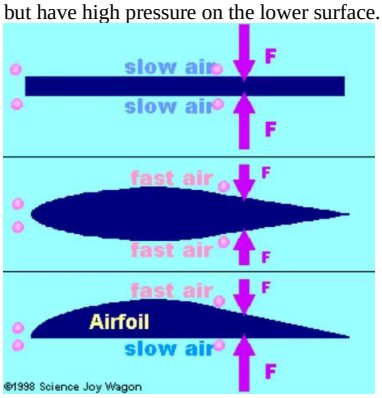


Figure 2. Physics of light, 2019
The coefficient of lift is given by:

$$C_L = \frac{L}{\frac{1}{2}\rho v^2 S} = \frac{L}{qS},$$

the section coefficient of lift is given by:

The current issue and full text archive of this journal is available at www.jraspublications.org/index.php/JRAS/issue/archive
Journal of Research in Administrative Sciences (JRAS)
V X(II), 1-9, ISSN: 2664-2433

$$c_l = \frac{1}{\frac{1}{2}\rho v^2 c},$$

As per Budarapu, & Natarajan, 2016 the lift coefficient of the section can be enhanced by changing the camber of the airfoil.
This results in the production of lift, where the low pressure produces a pull force, and the high pressure produces a push force. This is possible due to Bernoulli's Principle, which was discovered by the scientist Bernoulli, in which is stated that the pressure of a fluid declines at pointes where the speed of the fluid rises, with this he associated high speed flow with low pressure and low speed flow with high pressure.

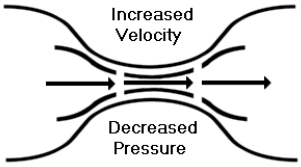


Figure 1. Aerofoil and lifts (Airfoils 2019)
This principle (Airfoils 2019) was used to initially to describe the changes in pressure of the fluid flowing within a pipe whose cross-sectional area is varied, which in the wide section going to gradually narrowing pipe moves at a low speed, which produces high pressure, but as the pipe narrows, it will try to accommodate the same amount of fluid. In turn increases the velocity of the fluid thus creating a decrease in pressure.

$$P + \frac{1}{2}\rho V^2 = \text{constant}$$

Figure 3. Theory of flight, 2019

2.2. Types of airfoil

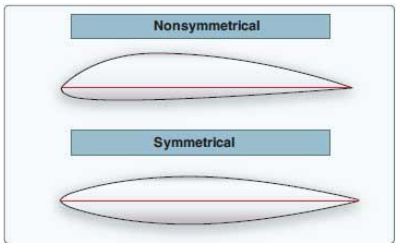


Figure 4. Aerofoil types. 2019

2.2.1. Symmetrical
Symmetrical airfoils a distinguished by having identical upper and lower surfaces. This kind of airfoil doesn't produce lift at zero angle of attack.
2.2.2. Non-symmetrical
This has different upper surface than the lower surface, but the upper surface has a greater curvature above the curve line than that of the lower surface. This would result in the chamber line to be different than that of the chord line, allowing the non-symmetrical to have the advantage of producing lift at zero angle of attack, allowing the airfoil to create lift at any angle of attack compared to a symmetrical airfoil, having a better lift to drag ratio. Disadvantage isn't also something they can't be avoided with the non-symmetrical design, like the center of pressure travels up to 20% of the chord line, which creates undesirable qualities on the airfoil, such as torque. It also has an increase in production cost.
Applications for airfoils are not only aircrafts specific, but some of the applications also include
- Spoilers
- Hydrofoils
- Helicopter rotors
- Propellers
- Wind turbines
- Vortex generators

2.3. Passive morphing airfoils
As per Du & Ang 2012 morphing technology is drawn for inspiration of for animals with the capabilities of flight, such as bats and birds. This technology can enable an aircraft to adapt to different conditions of flight by adjusting the wings shape to enable the enhancement of mission performance and optimize flight attitude controlling efficiency. As previously mentioned, the morphing airfoil is a concept proposed to eliminate the complexity a regular wing, by replacing different components such as flap, ailerons, elevator and rudders, this is to improve aerodynamic efficiency.

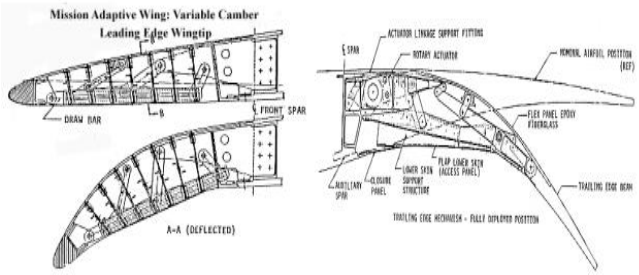


Figure 5. Aerofoil Mesh (Lu & Kota, 2003)
Applications of the morphing airfoil are vast due to its capability to adapt to various mission conditions, such of these applications are
- Missiles
- Unmanned Aerial Vehicles
- Military

2.4. Meso-Structures
As per (Yang & Chang, 2013) that meso structures are utilized widely in different applications of engineering applications. Specifically, honeycomb cells are the most commonly suggested cellular structures are an interest due to its beneficial properties mechanically and light weight characteristics. Honeycombs are prevalent in the design of light weight structures for various engineering applications.
The simplest geometry is a 2-dimensional array of polygons which pack to fill a plane area like hexagonal cells of the bee, which is why it is called honeycomb.
Such structures can be made in many ways first one is to press sheet material into a half-hexagonal profile and then glue the corrugated sheets together. More common way is to place glue in parallel strips on the flat sheets, and the sheets are arranged so that the glue bonds them together along the strips.
Some of the most common patterns include:
- Honeycomb

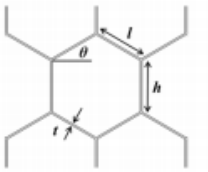


Figure 6. Honey comb structure (Heo and Kim, 2013)
- Re-entrant Honeycomb

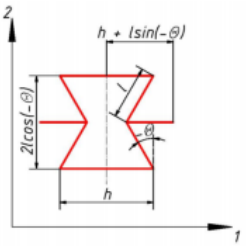


Figure 7. Auxetic structures (Ashjari, 2017)
There are different applications for Cellular solids, which include:
- Thermal insulation
- Packaging
- Structural
- Buoyancy

2.5. Material Selection
2.5.1. Al 6061 T6
This is a sub-category of the 6061 alloy, which is one of the most extensively used aluminum alloys, it is used in applications where high strength to low weight ratios are important such as aerospace applications, the main Al 6061 T6 has its characteristics is the way the base Al 6061 is treated, unlike the other Al 6061 variations, 6061 T6 has better machinability features, an improved anodizing response and comparable corrosion fighting properties.
The AL 6061 T6, is an alloy that is greatly appreciated due to its adaptable performing and all-around mechanical properties. The T6 is

the indication of the type of tempering treatment process that the aluminum alloy type underwent.

2.5.1.1. Tempering treatment process

2.5.1.1.1. First step (Heating)

The alloy is going to be submerge into a solution that has a steady temp of 527 degrees Celsius, the alloy pieces will remain in the solution for an hour until the it is going to be submerged in cold water, the initial hour is for the dissolving of the alloying elements in the aluminum, which the water quenching results in the mitigation of the precipitation of the individual alloying elements, on which will happen if the alloy is left to cool gradually.

2.5.1.1.2. Second step (Aging process)

The second step is done using different kinds of methods which would include the process of raising the temperature to 177 degrees Celsius, which is done for 1-18 hours, with the duration being specific to the shape, size or kind of application.

2.5.1.2. Why Al 6061 T6?

Al 6061 T6 is the one with the highest tensile strength out of all the 6061 types, so it is typically used in applications where high strength to low weight ratios are required. Which include aircraft and aerospace applications, rifle components, vacuum chambers etc.

2.5.1.3. Al 6061 Mechanical Properties

Table 1. Al 6061 Mechanical Properties

| Property | Value | Unit |
|---|---|---|
| | Al 6061 T6 | |
| Elastic Modulus | 6.900000067e+10 | N/m^2 |
| Poisson's Ratio | 0.33 | N/A |
| Mass Density | 2700 | kg/m^3 |
| Yield Strength | 275000000.9 | N/m^2 |

2.5.2. Glass Fiber Reinforced Polymer

Glass fiber Reinforced Polymer (GFRP) is a heavy-duty composite that has been a proven alternative to other materials such as steel, giving structures a better longevity at a lower cost.

GFRP has a high strength and corrosion proof glass fiber, which is integrated and coated with extremely durable polymer-based epoxy rosin. It has unique properties which is ideal for any environment that is harsh and corrosive environment, being resistant to moisture and is highly resistant to chemicals with acid and alkaline base.

GFRP doesn't contain any metal or any conductive material, which makes the material non-conductive and won't hamper or cause interference with string magnetic fields, which important in an aircraft, as conductivity may cause interference with the instruments on board the aircraft.

It is also very light, accounting to at least 9 times less than the weight of metal, which makes it easier to travel and easier to handle. Working with the material is easy due to its workable material properties.

2.5.2.1. GFRP Mechanical Properties

Table 2. GFRP Mechanical Properties

| Property | Value | Unit |
|---|---|---|
| | GFRP | |
| Elastic Modulus | 1.1551e+10 | N/m^2 |
| Poisson's Ratio | 0.257 | N/A |
| Mass Density | 1800 | kg/m^3 |
| Yield Strength | 250000000 | N/m^2 |

## 3. Aims and objective of the study

- Cellular pattern design
- Investigation of the behavior of the cellular patterns under static and aerodynamic loads with the use of Solidworks
- Structural analysis on the airfoil configurations
- CFD analysis on the airfoil configurations
- FSI on the airfoil configurations
- Deducing which Material and Structure is desirable

## 4. Methodology

This is the way the project was planned and handled.

- Literature review
- Airfoil
  - Types
  - Applications
  - Passive morphing airfoils
- Meso-structures
  - Honeycomb
- Materials
  - Al 6061 T6
  - Glass Fiber Reinforced Polymer (GFRP)
- Theoretical Background
- Calculations
- Pattern Design
- Airfoil Modelling
- Analysis
  - Structural Analysis (FEA)
    - Displacement
    - Stress (Von-Misses)
  - Computational Fluid Dynamics
    - Relative Pressure
    - Velocity
    - Exported Pressure Loads
  - Fluid-Structure analysis
    - Displacement
    - Stress (Von-Misses)
-

## 4. Theoretical background

4.1. In-plane Effective Moduli

(Heo and Kim, 2013) CMT or Cellular Material Theory is hugely influencing the description of the hexagonal honeycomb's elastic behavior, where the in-plane elastic moduli of honeycombs are given by:

$$E_{xx} = E_s(\frac{t}{l})^3 \frac{cos\theta}{(\frac{h}{l} + sin\theta)sin^2\theta}$$

$$E_{yy} = E_s(\frac{t}{l})^3 \frac{(\frac{h}{l} + sin\theta)}{cos^3\theta}$$

4.2. In-Plane Effective Strain

CMT uses the standard beam theory to provide a yield point for the honeycomb, as a function for a material' strength over a materials linear elastic range.

The maximum in-plane effective strain on which he cellular structures can withstand deformation without local cell wall failure when subjected to in-plane loading are given by:

$$(E_{xx})^{Yield} = \frac{\sigma^{yield}}{E_{xx}}(\frac{t}{l})^2 \frac{1}{2(\frac{h}{l} + sin\theta)|sin\theta|}$$

$$(E_{yy})^{Yield} = \frac{\sigma^{yield}}{E_{yy}}(\frac{t}{l})^2 \frac{1}{cos^2\theta}$$

4.3. Relative Density

The single most important structural characteristic of a cellular solid is its relative density p*/ps (p* is the density of the cellular solid, which is divided by he density of the material it is made of psi relative density of a honeycomb can be increased by further increasing the thickness of the cell walls, this resulting in the cell walls being more resistant to bending and cell wall collapse giving higher modulus and plateau stress. Density of the honeycomb is given by:

$$\rho^* = \rho \frac{\frac{t}{l}(\frac{h}{l} + 2)}{2cos\theta(\frac{h}{l} + sin\theta)}$$

$$Relative\ Density = \frac{\rho^*}{\rho}$$

Relative density of the Hybrid Honeycomb;

$$\frac{\rho^*}{\rho} = \frac{4l_at + 4h_at + 4l_ht + 0.5h_ht + 3t^2}{(2h_at - 2l_asin\theta)(2l_acos\theta + 2l_hcos\theta + 2t)}$$

4.4. Poisson's ratio

(Heo and Kim, 2013) Honey comb structures or geometries can be easily controlled from negative to positive Poisson's ratio by changing the angles from positive to negative.

$$v = \frac{sin\theta(\frac{h}{l} + \sin\theta)}{cos^2\theta}$$

## 5. Pattern Design

Considering the calculations made specific to the dimensions of the patterns, the design as is follows.

5.1. Honeycomb Pattern

honeycomb structure or geometries can be easily controlled from negative to positive Poisson's ratio by changing the angles. Considering different critical geometric parameters such as the cell angle (Ɵ), cell height (h), inclined cell wall length (l) and the wall thickness (t).

Table 3. Honeycomb dimensions

| | l (mm) | h (mm) | $\theta$ | t (mm) |
|---|---|---|---|---|
| Non-Auxetic Honeycomb | 20 | 20 | 30 | 1 |

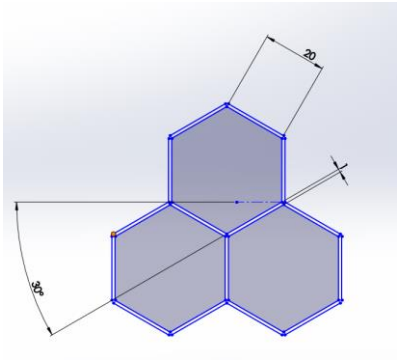


Figure 8. Honeycomb pattern

5.2. Auxetic Honeycomb

The design for the auxetic honeycomb is basically a re-entrant honeycomb, a honeycomb with negative angle.

Table 4. Auxetic Honeycomb Dimensions

| | l (mm) | h (mm) | $\theta$ | t (mm) |
|---|---|---|---|---|
| Auxetic Honeycomb | 20 | 40 | -30 | 1 |

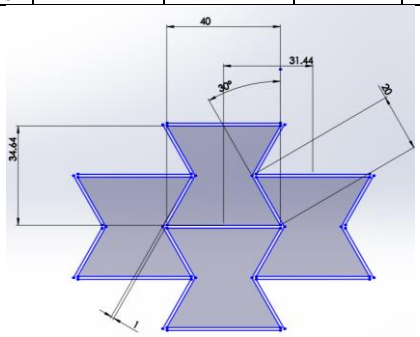


Figure 9. Auxetic Honeycomb

Following the cellular material theory both the auxetic and non-auxetic patterns were designed to have the same in-plane effective elastic modulus of 20 MPa both in the x and y directions.

5.3. Hybrid Honeycomb

The main motivation of the inclusion of the hybrid structure is the idea of zero Poisson's ratio. Which is achieved by mixing or integrating both structures with positive Poisson's ratio and negative Poisson's ratio resulting in a structure with zero Poisson's ratio.

Spadoni et al 2006) the main problem is that restraining the Poisson's ratio contraction or bulging, that a conventional and auxetic honeycomb experience during one dimensional morphing applications such as chord-, chamber- or span change in the non-morphing dimension, would lead into a substantial increase in the effective modulus in the morphing direction.

Table 5. Hybrid honeycomb dimensions

| | $l_a$ | $l_h$ | $h_a$ | $h_h$ | Θ | t |
|---|---|---|---|---|---|---|
| Hybrid Honeycomb | 20 | 20 | 40 | 20 | 30 | 1 |

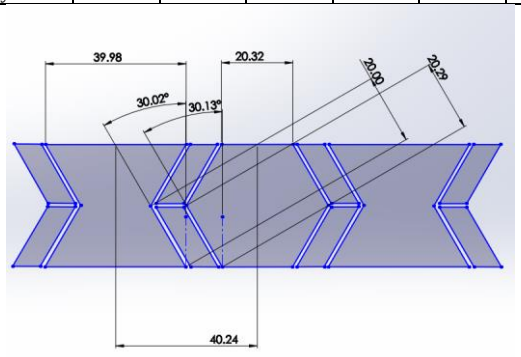


Figure 10. Hybrid Honeycomb

## 6. Airfoil Design

Following the literature, chambered airfoils are the main type suggested, the literature specifically recommended two chambered airfoils, the Eppler 420 and the Eppler 423, the reason is that these airfoils are highly chambered that they possess a good coefficient of lift to the coefficient of drag.

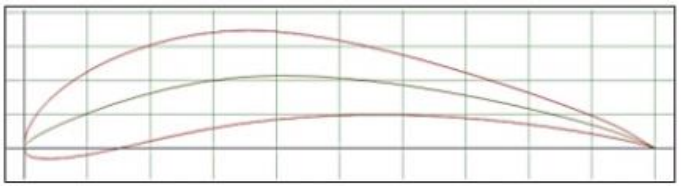

Figure 11. Eppler 420 (Nair, 2015)

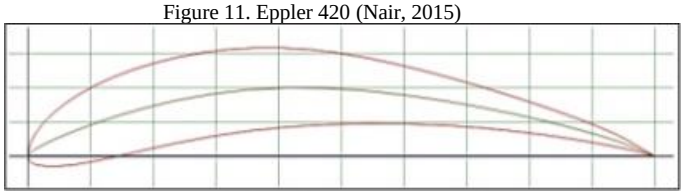

Figure 12. Eppler 423 (Nair, 2015)

When putting the two airfoils in contrast to one another, (Nair, 2015) the Eppler 420 had better values, the theoretical calculations from the literature show the same outcome, the 420 produced more lift and less drag, for this result, the Eppler 420 is the airfoil of choice.

6.1. Airfoil Modelling

The dimensions of the model are taken from the NACA database and then the coordinates are mapped in solid works. The geometric details are as mentioned in (Budarapu & Natarajan, 2016).

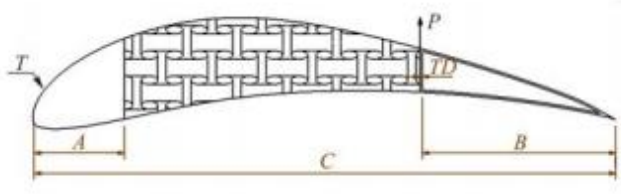


Figure 13. Auxetic Aerofoil (Budarapu & Natarajan, 2016).

Chord length (c) = 700 mm, A = 110 mm, B = 235 mm, Skin thickness = 1 mm, Out of plane thickness = 19 mm, Trailing edge profile (TD) = 2.54 mm. Then the patterns are mapped into the airfoil following the skin thickness of 1mm.

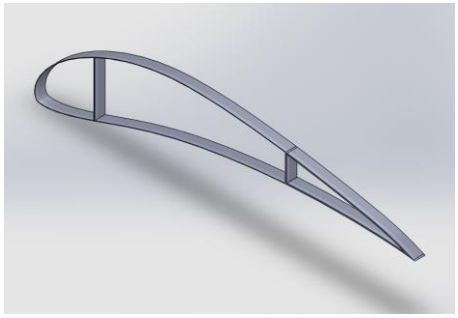

Figure 14. 3d model of airfoil section

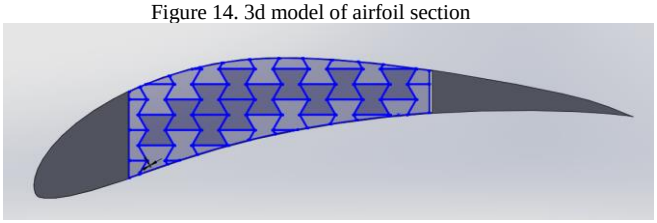

Figure 15. Mapping the Patterns

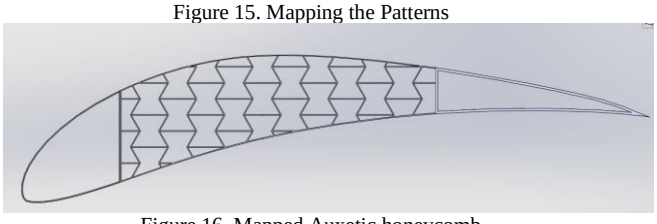

Figure 16. Mapped Auxetic honeycomb

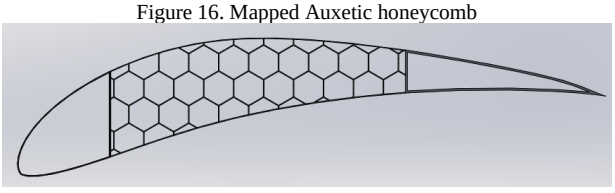

Figure 17. Mapped Honeycomb

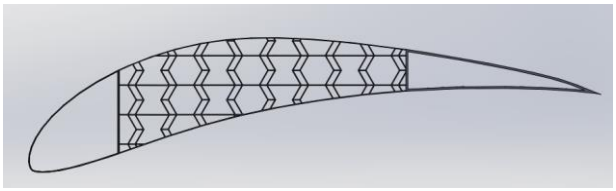

Figure 18. Mapped Hybrid honeycomb

## 7. Analysis and Results

7.1. Structural Analysis

3D Structural models is required to investigate the characteristics of an Airfoil, this is because the FSI analysis that is going to be done on the airfoil requires a 3D solid element. This is conducted to understand and evaluate the compliance of the pattern or configurations, and the find the displacements of each pattern on the specific given range of loadings.

The structural analysis is done on each pattern with two distinct material, one Al 6061 T6 and Glass Fiber Reinforced Polymer.

Assumptions

- Materials would be Al 6061 T6 and GFRP
- The fixture would be on the leading edge of the airfoil section

The concentrated force will be applied between the core and the trailing edge.

7.1.1. Auxetic Honeycomb

7.1.1.1. Displacement

7.1.1.1.1. 5N

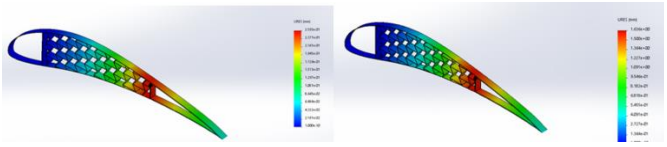

Figure 19. Displacement at 5N for Al 6061 T6 and GFRP respectively

7.1.1.1.2. 80N

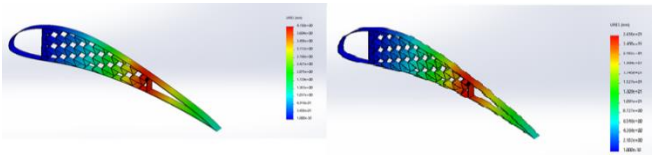

Figure 20. Displacement at 80N for Al 6061 T6 and GFRP respectively

7.1.1.1.3. 150N

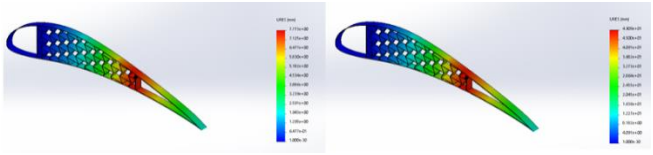

Figure 21. Displacement at 150N for Al 6061 T6 and GFRP respectively

7.1.1.2. Stress (Von-Misses)

7.1.1.2.1. 5N

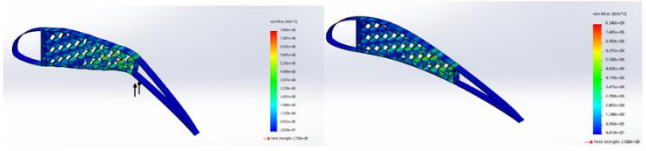

Figure 22. Stress at 5N for Al 6061 T6 and GFRP respectively

7.1.1.2.2. 80N

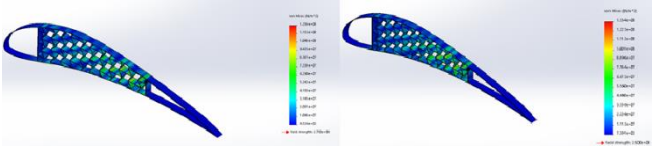

Figure 23. Stress at 80N for Al 6061 T6 and GFRP respectively

7.1.1.2.3. 150N

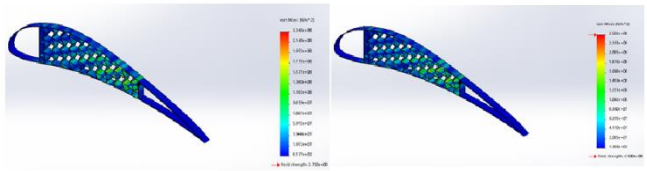

Figure 24. Stress at 150N for Al 6061 T6 and GFRP respectively

7.1.2. Non-Auxetic Honeycomb

7.1.2.1. Displacement

7.1.2.1.1. 5N

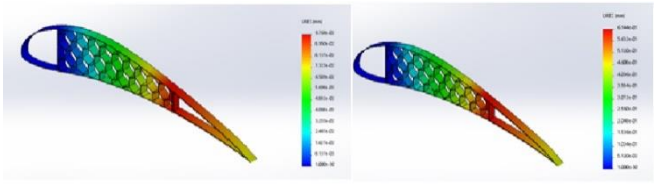

Figure 25. Displacement at 5N for Al 6061 T6 and GFRP respectively

7.1.2.1.2. 80N

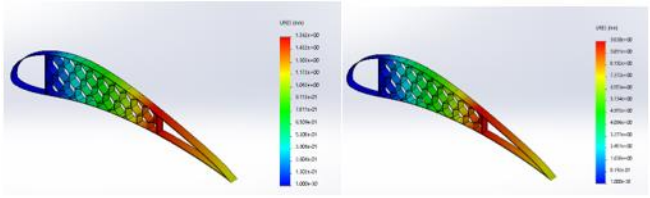

Figure 26. Displacement at 80N for Al 6061 T6 and GFRP respectively

7.1.2.1.3. 150N

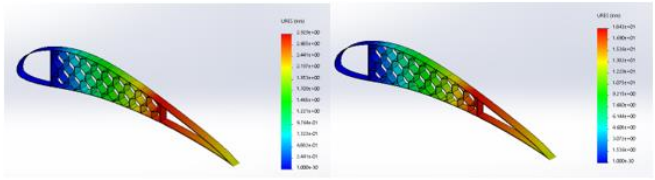

Figure 27. Displacement at 150N for Al 6061 T6 and GFRP respectively

7.1.2.2. Stress (Von-Misses)

7.1.2.2.1. 5N

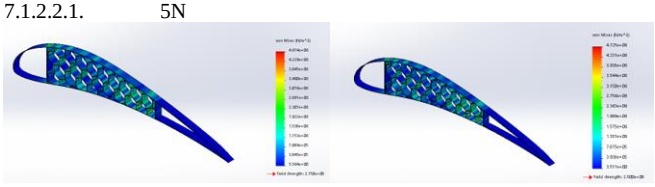

Figure 28. Stress at 5N for Al 6061 T6 and GFRP respectively

7.1.2.2.2. 80N

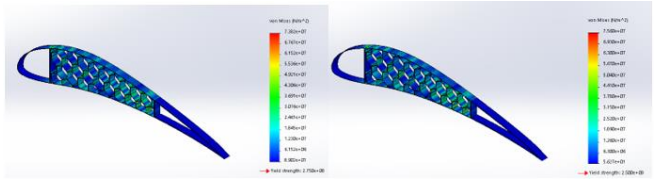

Figure 29. Stress at 80N for Al 6061 T6 and GFRP respectively

7.1.2.2.3. 150N

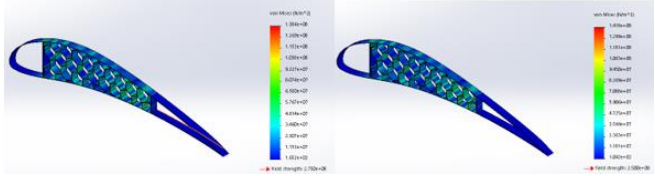

Figure 30. Stress at 80N for Al 6061 T6 and GFRP respectively

7.1.3. Non-Auxetic Honeycomb

7.1.3.1. Displacement

7.1.3.1.1. 5N

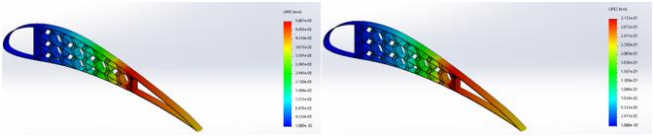

Figure 31. Displacement at 5N for Al 6061 T6 and GFRP respectively

7.1.3.1.2. 80N

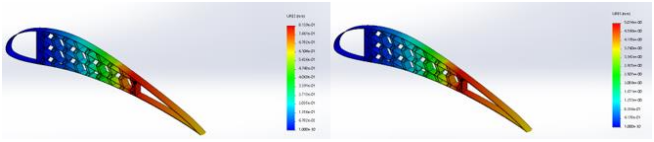

Figure 32. Displacement at 80N for Al 6061 T6 and GFRP respectively

7.1.3.1.3. 150N

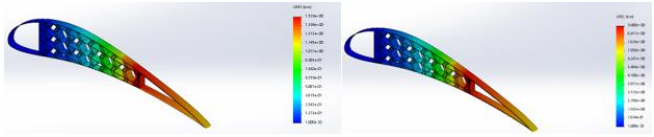

Figure 33. Displacement at 150N for Al 6061 T6 and GFRP respectively

7.1.3.2. Stress (Von-Misses)

7.1.3.2.1. 5N

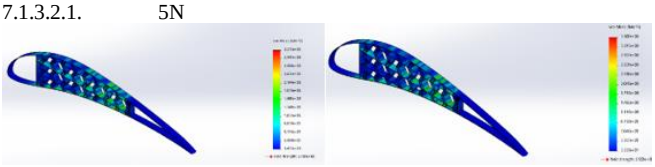

Figure 34. Stress at 5N for Al 6061 T6 and GFRP respectively

7.1.3.2.2. 80N

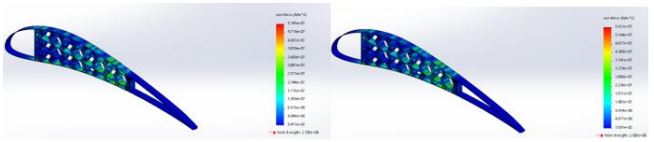

Figure 35. Stress at 80N for Al 6061 T6 and GFRP respectively

7.1.3.2.3. 150N

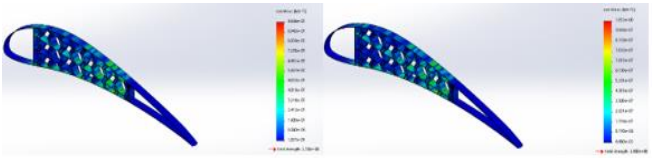

Figure 36. Stress at 150N for Al 6061 T6 and GFRP respectively

7.1.4. Results

7.1.4.1. Displacement

Table 6. Tabulated results for displacement

| Displacement (mm) | | |
|---|---|---|
| Pattern | Al 6061 T6 | GFRP |
| Auxetic Honeycomb | 7.78E+00 | 4.91E+01 |
| Non-Auxetic Honeycomb | 2.93E+00 | 1.84E+01 |
| Hybrid Honeycomb | 1.53E+00 | 9.40E+00 |

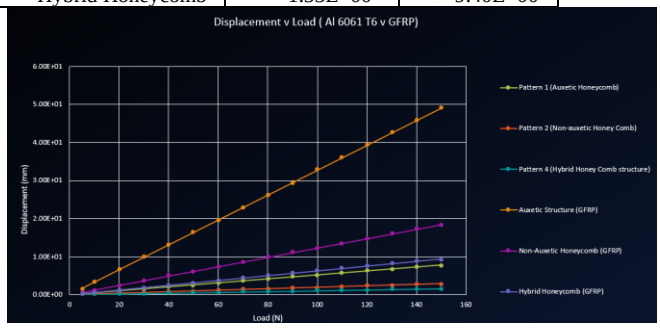


Figure 37. Stress vs load

The displacement results show that the auxetic honeycomb shows a high amount of displacement compared to the other patterns, meaning that the hybrid honeycomb is stiffer than the other patterns. GFRP has 531.105% increase in displacement at the same load, understanding this the GFRP material is a much more flexible material.

7.1.4.2. Stress

7.1.4.2.1. Results

Table 7. Tabulated results for stress

| Max Stress (Pa) | | |
|---|---|---|
| Pattern | Al 6061 T6 | GFRP |
| Auxetic Honeycomb | 2.36E+08 | 2.50E+08 |
| Non-Auxetic Honeycomb | 1.38E+08 | 1.42E+08 |
| Hybrid Honeycomb | 9.65E+07 | 1.05E+08 |

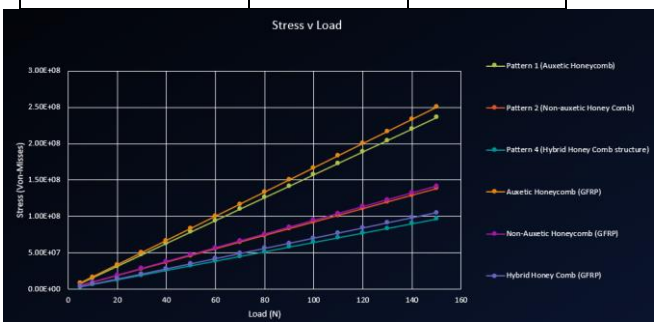


Figure 38. Displacement vs load

The results show that there is more local stress on the auxetic honeycomb compared to the other patterns. The hybrid honeycomb shows more restraint to stress compared to the other patterns. The GFRP material is having an increase in local stress by 5.88% compared to the Al 6061 T6.

This static analysis is conducted to evaluate the compliance of the three patterns, and to find the behavior of the patterns on a given scenario, in this case different loading cases. The maximum applied load on the patterns is 150N, the displacement and the stresses of the patterns and their consequent materials are shown on table 10 and 11.

7.2. Computational Fluid Dynamics Analysis

The reason this analysis is done is to get the interaction of the fluid with the airfoil, which in this case is air, by considering assumptions. then these interactions would be considered as aerodynamic loads that surround the airfoil and these aerodynamic loads will be transferred to the structural model for the Fluid Interaction analysis.

Assumptions:

- Using the relative pressure contours of the free stream.
- The reference pressure of the fluid domain is 1 atm
- The dimensions of the flow field are 8.5 m horizontal and 7 m vertical
- The angle of attack will be 2 deg and 14 deg
- The inlet velocity will be Mach of 0.45
- The reference pressure is affecting the pressure load on the airfoil
- Using the aerodynamic loads to be exported to the structural model of the airfoil for FSI analysis.

Since the analysis only requires the relative pressure contours, the velocity contours are going to be included to see if the airfoil configurations produce lift, 2 angles of attacks are going to be considered for two different working conditions, one for cruising ($2^0$) and for takeoff ($14^o$).

7.2.1. Angle of Attack $2^o$

7.2.1.1. Auxetic Honeycomb

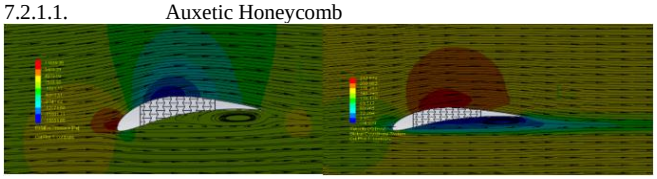

Figure 39. CFD of auxetic honeycomb, relative pressure and velocity respectively

7.2.1.2. Non-Auxetic Honeycomb

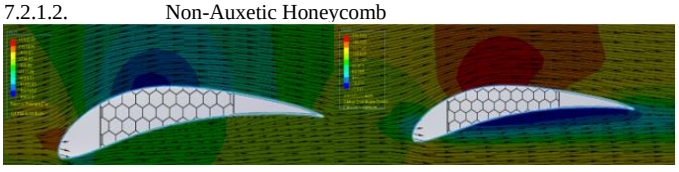

Figure 40. CFD of non-auxetic honeycomb, relative pressure and velocity respectively

7.2.1.3. Hybrid Honeycomb

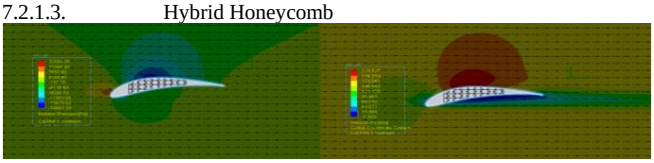

Figure 41. CFD of Hybrid honeycomb, relative pressure and velocity respectively

7.2.2. Angle of Attack 14º

7.2.2.1. Auxetic Honeycomb

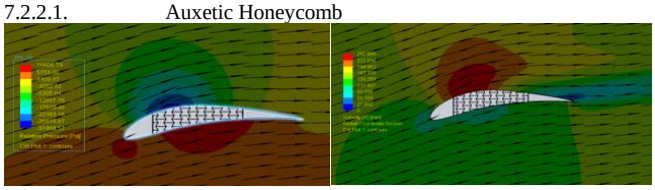

Figure 42. CFD of auxetic honeycomb, relative pressure and velocity respectively

7.2.2.2. Non-Auxetic Honeycomb

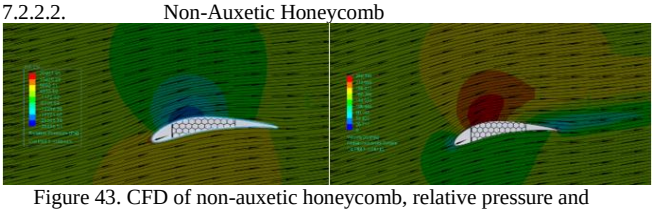

Figure 43. CFD of non-auxetic honeycomb, relative pressure and velocity respectively

7.2.2.3. Hybrid Honeycomb

Figure 44. CFD of Hybrid honeycomb, relative pressure and velocity respectively

All the airfoil configurations adhere to the basic requirements such as having low pressure on the upper skin of the airfoil and high pressure on the lower skin of the airfoil, this is the results of having high velocity on the upper skin and low velocity on the lower skin of the airfoil.

Specifically, the relative pressure is going to be taken as aerodynamic loads and are going to be transferred to the structural model of the airfoil and to be taken as pressure loads surrounding the airfoil, then the structural model will be analyzed again with the consideration of the pressure loads surrounding the airfoil.

7.3. Fluid-Structure Interaction

This analysis is basically the interaction of a deformable structure with either internal or external fluid flow, in this study air is the fluid and is surrounding the airfoil, this kind of analysis can either be stable or oscillatory, but in this study the airfoil is stable, as the displacement and the stress would only be taken.

The fluid flow data of both angle of attack 2º and 14º will be implemented with the structural model of the airfoil for each configuration as aerodynamic loads, then the displacements and the stresses of one another will be compared.

7.3.1. Angle of attack 2º

7.3.1.1. Al 6061 T6

7.3.1.1.1. Auxetic Honeycomb

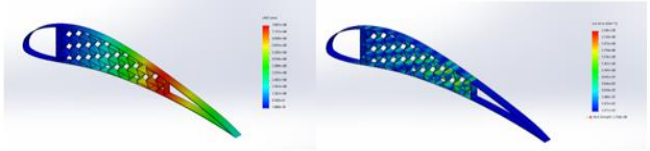

Figure 45. FSI of auxetic honeycomb (Al 6061 T6), both displacement and stress, respectively

7.3.1.1.2. Non-Auxetic Honeycomb

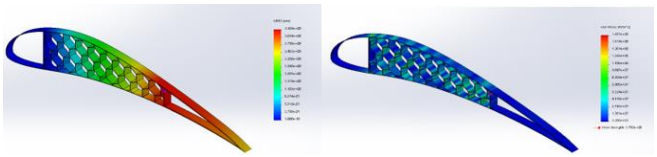

Figure 46. FSI of non-auxetic honeycomb (Al 6061 T6), both displacement and stress, respectively

7.3.1.1.3. Hybrid Honeycomb

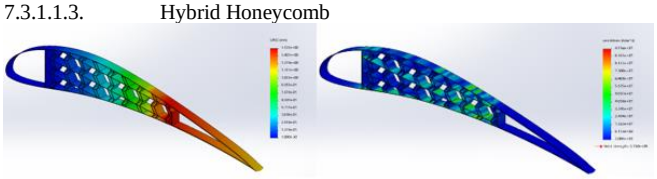

Figure 47. FSI of hybird honeycomb (Al 6061 T6), both displacement and stress, respectively

7.3.1.2. GFRP

7.3.1.2.1. Auxetic Honeycomb

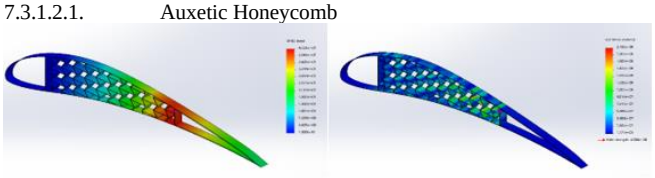

Figure 48. FSI of auxetic honeycomb (GFRP), both displacement and stress, respectively

7.3.1.2.2. Non-Auxetic Honeycomb

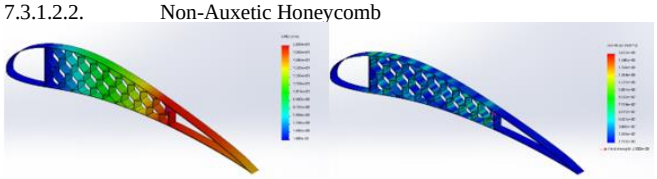

Figure 49. FSI of non-auxetic honeycomb (GFRP), both displacement and stress, respectively

7.3.1.2.3. Hybrid Honeycomb

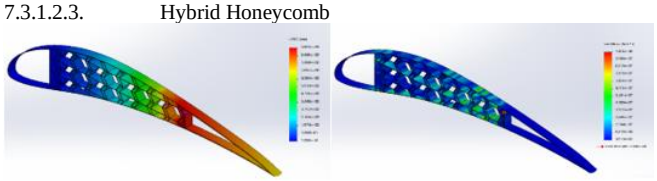

Figure 50. FSI of hybrid honeycomb (GFRP), both displacement and stress, respectively

7.3.2. Angle of attack 14º

7.3.2.1. Al 6061 T6

7.3.2.1.1. Auxetic Honeycomb

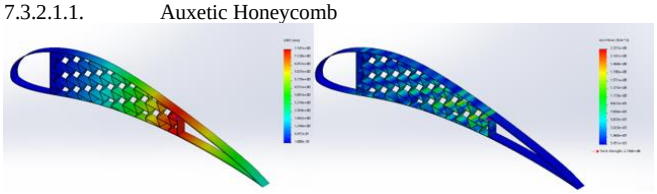

Figure 51. FSI of auxetic honeycomb (Al 6061 T6), both displacement and stress, respectively

7.3.2.1.2. Non-Auxetic Honeycomb

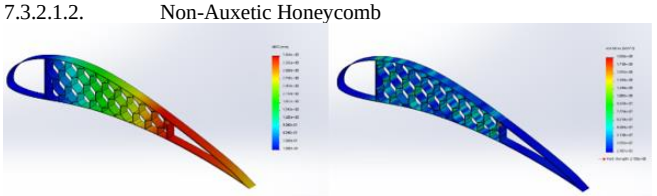

Figure 52. FSI of non-auxetic honeycomb (Al 6061 T6), both displacement and stress, respectively

7.3.2.1.3. Hybrid Honeycomb

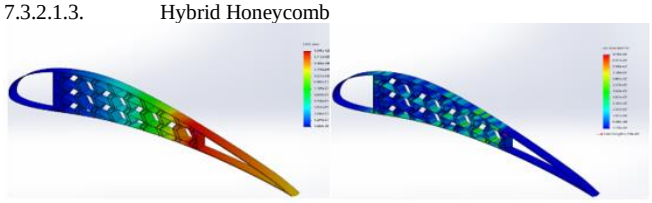

Figure 53. FSI of hybird honeycomb (Al 6061 T6), both displacement and stress, respectively

7.3.2.2. Al 6061 T6

7.3.2.2.1. Auxetic Honeycomb

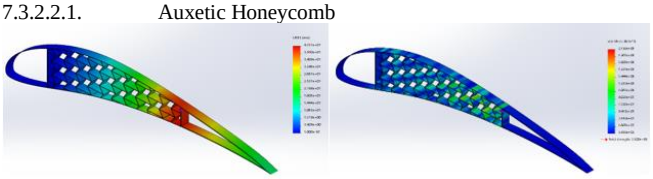

Figure 54. FSI of auxetic honeycomb (GFRP), both displacement and stress, respectively

7.3.2.2.2. Non-Auxetic Honeycomb

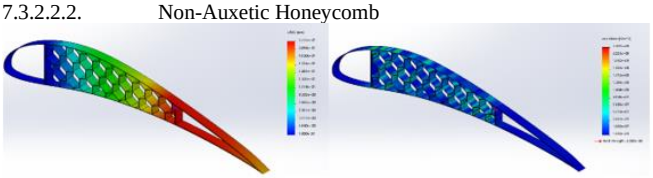

Figure 55. FSI of non-auxetic honeycomb (GFRP), both displacement and stress, respectively

7.3.2.2.3. Hybrid Honeycomb

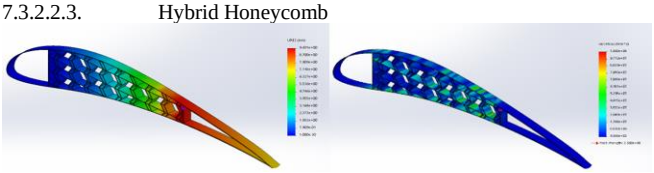

Figure 56. FSI of hybrid honeycomb (GFRP), both displacement and stress, respectively

Table 8. Tabulated results for AoA 2°

| Pattern | AoA 2° | | | |
|---|---|---|---|---|
| | Al 6061 T6 | | GFRP | |
| | Disp. (mm) | Stress (Pa) | Disp. (mm) | Stress (Pa) |
| AHC | 7.807 | $2.16x10^8$ | 43.3 | $2.16x10^8$ |
| NAHC | 3.309 | $1.66x10^8$ | 20.4 | $1.85x10^8$ |
| HHC | 1.535 | $9.73x10^7$ | 9.46 | $1.06x10^8$ |

Table 9. Tabulated results for AoA 14°

| Pattern | AoA 14° | | | |
|---|---|---|---|---|
| | Al 6061 T6 | | GFRP | |
| | Disp. (mm) | Stress (Pa) | Disp. (mm) | Stress (Pa) |
| AHC | 7.767 | $2.36x10^8$ | 43.31 | $2.17x10^8$ |
| NAHC | 3.624 | $1.87x10^8$ | 22.3 | $2.21x10^8$ |
| HHC | 1.541 | $9.73x10^7$ | 9.49 | $1.06x10^8$ |

It can be seen that the auxetic structure has the highest displacement and stress after applying the aerodynamic loads from the Computational fluid dynamics, with having values for displacement and stress respectively, 7.807 mm and 216.3 MPa for Al 6061 T6 and, 43.25 mm and 216.3MPa for GFRP at the angle of attack of 20 and for the angle of attack 140, 7.767mm and 235.7 MPa for Al 6061 T6 and, 43.31 mm and 216.6MPa for GFRP.

## 8. Conclusion

The maximum displacement and local stresses at the given loads are investigated to understand and identify the behavior of Meso-structures being integrated with in a morphing airfoil.

The results show that the auxetic structure possesses a higher local stress and displacement at the maximum given load of 150N than the other patterns. Between the two materials Al 6061 T6 and GFRP, Al 6061 T6 has low local stress than that of the GFRP material, although the there is an average of 6.3% of difference in local stress, GFRP has more displacement than that of the Al 6061 T6, which is better for passive morphing airfoil applications requiring large deformations during flight conditions. The hybrid honeycomb is much more desirable in this study, as though even it has the least displacement compared to the other pattern Its local stress is much more desirable than the rest, providing more room for harsher or increased aerodynamic loading conditions that if applied on the other airfoil configurations may cause the structures to fail.

## 9. Further Scope

Further research can be done on this subject, specially the meso-structures that can be mapped into an airfoil. Some of these studies can include:

- Analyzing the patterns again, but with the design of the patterns to have the same bending stiffness
- Analyzing other applications for morphing wings, aside from aerospace applications
- Explore the possibility of designing a novel hybrid honeycomb pattern
- Explore other auxetic structures
- Analyze the morphing airfoil when extruding it to a full wing
- Understand the more theoretical equations for the hybrid honeycomb

## 10. References

i. Airfoils and Lift. (2019). Retrieved from http://www.aviation-history.com/theory/airfoil.htm

ii. Physics of flight. (2019). Ambition to fly: Making the dream a reality. Retrieved from https://ambitiontofly.wordpress.com/2011/10/30/physics-of-flight/

iii. Theory of Flight. (2019). Retrieved from http://web.mit.edu/16.00/www/aec/flight.html

iv. Airfoils – Airfoil Types. (2019). Helicopter Flight Training. Retrieved from https://www.danubewings.com/airfoils-airfoil-types/

v. Lu, K., & Kota, S. (2003). Design of Compliant Mechanisms for Morphing Structural Shapes. Journal of Intelligent *Material Systems and Structures, 14*(6):379-391.

vi. Heo, H., Ju, J., & Kim, D. (2013). Compliant cellular structures: Application to a passive morphing airfoil. *Composite Structures*, 106:560-569.

vii. Ashjari, M. (2017). Auxetic Materials Materials with Negative Poisson's Ratio. *Material Science & Engineering International Journal, 1*(2).

viii. Nair, P. (2015). Aerodynamics [Undergraduate]. Carlton University.

ix. Budarapu, P., Y. B. S., & Natarajan, R. (2016). Design concepts of an aircraft wing: composite and morphing airfoil with auxetic structures. *Frontiers of Structural and Civil Engineering, 10*(4):394-408.

x. Abbott, I., & Doenhoff, A. (1959). *Theory of Wing Sections*. [Place of publication not identified]: Dover Pubns

xi. Almgren, R. (1985). An isotropic three-dimensional structure with Poisson's ratio =?1. *Journal of Elasticity, 15*(4):427-430.

xii. Attard, D., & Grima, J. (2010). Modelling of hexagonal honeycombs exhibiting zero Poisson's ratio. *physica status solidi (b), 248*(1):52-59.

xiii. Balawi, S., & Abot, J. (2008). A refined model for the effective in-plane elastic moduli of hexagonal honeycombs. *Composite Structures, 84*(2):147-158.

xiv. Bezazi, A., Scarpa, F., & Remillat, C. (2005). A novel centresymmetric honeycomb composite structure. *Composite Structures, 71*(3-4):356-364.

xv. Chen, Y., & Fu, M. (2017). Mechanical Properties of a Novel Zero Poisson's Ratio Honeycomb. *Advanced Engineering Materials, 20*(2):1700452.

xvi. Dong, W., & Sun, Q. (2011). Airfoil Design and Numerical Analysis for Morphing Wing Structure. *Advanced Materials Research*, 228-229:169-173.

xvii. Du, S., & Ang, H. (2012). Design and Feasibility Analyses of Morphing Airfoil Used to Control Flight Attitude. Strojniški vestnik – *Journal of Mechanical Engineering, 58*(1):46-55.

xviii. Evans K. (1989). Tensile network microstructures exhibiting negative Poisson's ratios. *Journal of Physics D: Applied Physics, 22*(12):1870-1876.

xix. Gibson, L., & Ashby, M. (2010). *Cellular solids*. Cambridge: Cambridge Univ. Press

xx. Gonella, S., & Ruzzene, M. (2008). Homogenization and equivalent in-plane properties of two-dimensional periodic lattices. *International Journal of Solids and Structures, 45*(10):2897-2915.

xxi. Gong, X., Huang, J., Scarpa, F., Lium Y., & Leng, J. (2015). Zero Poisson's ratio cellular structure for two-dimensional morphing applications. *Composite Structures, 134*:384-392.

xxii. Ingrole, A., & Hao, A., (2017). Liang R. Design and modeling of auxetic and hybrid honeycomb structures for in-plane property enhancement. *Materials & Design, 117*:72-83.

xxiii. Ju, J., & Summers, J. (2011). Compliant hexagonal periodic lattice structures having both high shear strength and high shear strain. *Materials & Design, 32*(2):512-524.

*xxiv.* Kota, S., Hetrick, J., Osborn, R., Paul, D., Pendleton, E., …, & Flick, P. (2003). Design and application of compliant mechanisms for morphing aircraft structures. *Smart Structures and Materials. Industrial and Commercial Applications of Smart Structures Technologies.*

xxv. Li, D., Zhao, S., Ronch, A., Xiang, J., Drofelnik, J., …, & Li, Y. (2018). A review of modelling and analysis of morphing wings. *Progress in Aerospace Sciences*, *100*:46-62.

xxvi. Lira, C., Innocenti, P., & Scarpa, F. (2009). Transverse elastic shear of auxetic multi re-entrant honeycombs. *Composite Structures*, *90*(3):314-322.

xxvii. MacCormick, B. (1995). *Aerodynamics, aeronautics, and flight mechanics*. New York [etc.]: J. Wiley & Sons

xxviii. Masters, I., & Evans, K. (1996). Models for the elastic deformation of honeycombs. *Composite Structures*, *35*(4):403-422.

xxix. Namgoong, H., Crossley, W., & Lyrintzis, (2007). A. Aerodynamic Optimization of a Morphing Airfoil Using Energy as an Objective. *AIAA Journal*, *45*(9):2113-2124.

xxx. Olympio, K., & Gandhi, F. (2009). Zero Poisson's Ratio Cellular Honeycombs for Flex Skins Undergoing One-Dimensional Morphing. *Journal of Intelligent Material Systems and Structures*, *21*(17):1737-1753.

xxxi. Ou, Y., Zhu, D., Zhang, H., Huang, L., Yao, Y., … Li, G. (2016). Mechanical Characterization of the Tensile Properties of Glass Fiber and Its Reinforced Polymer (GFRP) Composite under Varying Strain *Rates and Temperatures. Polymers*, *8*(5):196.

xxxii. Pope A. (1951). *Basic wing and airfoil theory*. 1st ed. New york: McGraw-Hill Book Company, Inc.

xxxiii. Prall, D., & Lakes, R. (1997). Properties of a chiral honeycomb with a poisson's ratio of — 1. *International Journal of Mechanical Sciences*, *39*(3):305-314.

xxxiv. Santulli, C., & Langella, C. (2016). Study and development of concepts of auxetic structures in bio-inspired design. *International Journal of Sustainable Design*, *3*(1):20.

xxxv. Spadoni, A., & Ruzzene, M. (2007). Numerical and experimental analysis of the static compliance of chiral truss-core airfoils. *Journal of Mechanics of Materials and Structures*, *2*(5):965-981.

xxxvi. Spadoni, A., & Ruzzene, M. (2007). Static Aeroelastic Response of Chiral-core Airfoils. *Journal of Intelligent Material Systems and Structures*, *18*(10):1067-1075.

xxxvii. Spadoni, A., Ruzzene, M., & Scarpa, F. (2006). Dynamic Response of Chiral Truss-core Assemblies. Journal of Intelligent *Material Systems and Structures*, *17*(11):941-952.

xxxviii. Vos, R., & Barrett, R. (2011). Mechanics of pressure-adaptive honeycomb and its application to wing morphing. *Smart Materials and Structures*, *20*(9):094010.

xxxix. Xu, M., Xu, Z., Zhang, Z., Lei, H., Bai, Y., & Fang, D. (2019). Mechanical properties and energy absorption capability of AuxHex structure under in-plane compression: Theoretical and experimental studies. *International Journal of Mechanical Sciences*, *159*, 43-57.

xl. Yang, C., Vora, H., & Chang, Y. (2018). Behavior of auxetic structures under compression and impact forces. *Smart Materials and Structures*, *27*(2):025012.